Deliverable 3.5: Performance of ancillary services provision from WFs connected to DR-HVDC

Saborío-Romano, Oscar; Göksu, Ömer

Publication date:
2018

Document Version
Publisher's PDF, also known as Version of record

PROMOTioN
PROGRESS ON MESHED HVDC OFFSHORE TRANSMISSION NETWORKS

Deliverable 3.5: Performance of ancillary services provision from WFs connected to DR-HVDC

PROMOTioN – Progress on Meshed HVDC Offshore Transmission Networks
Mail info@promotion-offshore.net
Web www.promotion-offshore.net

This result is part of a project that has received funding form the European Union's Horizon 2020 research and innovation programme under grant agreement No 691714.

DOCUMENT INFO SHEET

Document Name:	Deliverable 3.5: Performance of ancillary services provision from WFs connected to DR-HVDC
Responsible partner:	DTU (Technical University of Denmark)
Work Package:	WP 3
Work Package leader:	Ömer Göksu (DTU)
Task:	3.2 General control algorithms (M09-M24)
Task lead:	Ömer Göksu (DTU)

DISTRIBUTION LIST

PROMOTioN partners, European Commission

APPROVALS

	Name	Company
Validated by:	Kees Koreman	TenneT
	Dirk Van Hertem	KUL
Task leader:	Ömer Göksu	DTU
WP Leader:	Ömer Göksu	DTU

DOCUMENT HISTORY

Version	Date	Main modification	Author
1	26/09/2017	Proposal for the structure of the document	Oscar Saborío-Romano (DTU)
2	13/11/2017	Initial draft; document structure changed	Oscar Saborío-Romano (DTU)
3	05/12/2017	Full draft for revision	Oscar Saborío-Romano (DTU)
4	16/01/2018	Final version	Oscar Saborío-Romano (DTU)

WP Number	WP Title	Person months	Start month	End month
WP3	Wind Turbine – Converter Interaction	269	3	42

Deliverable Number	Deliverable Title	Type	Dissemination level	Due Date
D3.5	Performance of ancillary services provision from WFs connected to DR-HVDC	Report	Public	24

CONTENT

Document info sheet i

Distribution list i

Approvals i

Document history i

1. Introduction 2

2. Modelling and control 3

2.1. Onshore frequency support 5

2.2. Onshore power oscillation damping 8

3. Simulation results 10

3.1. Onshore frequency support 10

3.1.1 Onshore over-frequency event 11

3.1.2 Onshore under-frequency event 16

3.2. Onshore power oscillation damping 21

4. Conclusions and recommendations 23

4.1. Conclusions 23

4.2. Recommendations for future work 23

Bibliography 24

1. INTRODUCTION

This report is part of Task 3.2: General Control Algorithms, which includes the specification of control strategies, definition of test cases, implementation of control strategies and test cases, and stability assessment and tuning of controllers.

This document covers the assessment of the capabilities of offshore wind farms (offshore WFs, OWFs) to contribute in the provision of ancillary services to onshore alternating-current (AC) networks by means of active power modulation, when connected through high-voltage direct-current (HVDC) links having diode rectifier (DR) offshore terminals and voltage source converter (VSC) onshore terminals. In doing so, the compatibility of corresponding higher-level controls previously devised for VSC-HVDC-connected OWFs is examined. Through such controls, the OWFs modify their active power output according to the onshore signals directly communicated to them, to contribute in the provision of onshore frequency support or onshore power oscillation damping. Other ancillary services to onshore AC networks[1] are out of the scope of this document, as they are provided by the (HVDC) onshore terminals mainly and/or they are not relevant in the studied system. Such services and any contribution of the onshore terminals in the provision of the studied services are left to be considered in Work Package 2, as are also the impact and benefit of the studied services on the onshore synchronous area stability.

The document is organised as follows. In Section 2, the investigated system is described, the studied services and main control algorithms are detailed, and the three different wind turbine (WT) overloading methods are explained. In Section 3, the considered cases are described, and corresponding simulation results are presented and discussed. Finally, concluding remarks and recommendations for future work are made in Section 4.

1 such as reactive power/voltage control/support, avoiding loss of synchronism, black start and restoration, DC transmission reserve, and DC power flow control

This project has received funding from the European Union's Horizon 2020 research and innovation programme under grant agreement No 691714.

2. MODELLING AND CONTROL

A simplified block diagram of the OWF (group) functionality is shown in Figure 2-1. The developed controls for the OWF (group) to contribute in the provision of ancillary services to an onshore AC network are based on the OWF active power controls developed in [L. Zeni 2015; J. N. Sakamuri *et al.* 2017] for OWFs connected to HVDC via VSCs. In normal operation mode (DR configuration with continuous conduction), an OWF (group) contributes in the provision of ancillary services to the onshore AC network by means of its active power control subsystem, which modifies, amongst others, the value of its active power reference input [PROMOTioN 2017; PROMOTioN 2016; L. Zeni 2015].

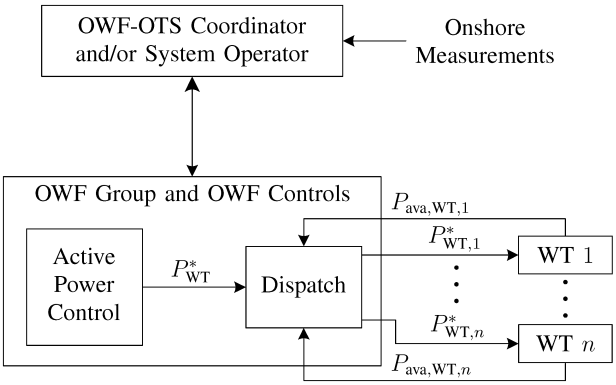

Figure 2-1: Simplified block diagram of the OWF (group) functionality for providing ancillary services to an onshore AC network

Active power reference signals are then dispatched to each WT, $P^*_{\mathrm{WT},i}$, taking into account their available active power, $P_{\mathrm{ava,WT},i}$, while ensuring that gain and phase shifts caused by the WT controllers are cancelled out, that the requirements for normal operation are fulfilled (e.g., offshore frequency and voltage maintained within their required operational ranges), and that the overall OWF (group) response is as required. The studied schemes rely on the direct communication of the necessary onshore measurements by means of signals sent by the coordinator of the OWF (group) and offshore transmission system (OWF-OTS coordinator) or the system operator. The study of the actual capability of the OWF (group) to provide such services has been prioritised over e.g., the study of their impact and benefit on the onshore synchronous area stability [PROMOTioN 2017; PROMOTioN 2016; L. Zeni 2015].

Figure 2-2 shows an overview of the investigated system and of the associated control structure. The system is comprised of an OWF connected to an onshore AC network by means of a monopolar HVDC link and is based on those studied in [R. M. Blasco-Giménez *et al.* 2011; S. I. Bernal-Pérez 2015; S. I. Bernal-Pérez *et al.* 2015]. Balanced/symmetric operation has been assumed. The WF is modelled as an aggregated type-4 (full-converter) WT. Its DC link dynamics have not been considered, and the corresponding voltage have thus been assumed constant (ideally regulated). The front-end VSC injects the WT/WF output active power, $P = P_{\mathrm{WT}}$, into the offshore AC network through the WT step-up transformer, $\mathrm{T_W}$.

This project has received funding from the European Union's Horizon 2020 research and innovation programme under grant agreement No 691714.

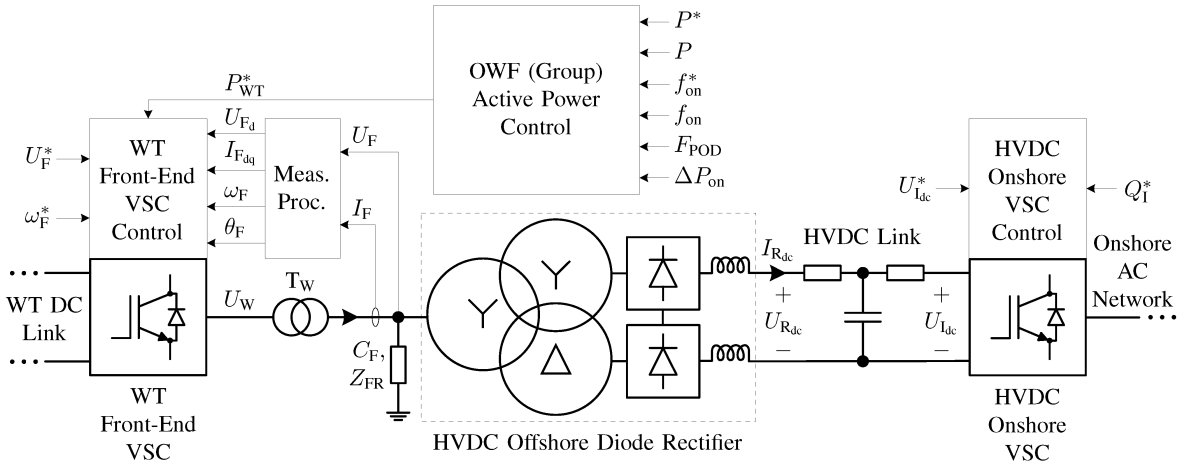

Figure 2-2: Overview of the investigated system and control structure

The HVDC offshore terminal is modelled as a diode-based (uncontrolled) 12-pulse rectifier (diode rectifier, DR), with corresponding reactive power compensation, C_{F}, and filter bank, Z_{FR}, on its AC side. The submarine cables connecting the HVDC terminals are modelled using the equivalent T circuit. The HVDC onshore terminal consists of a VSC, which controls the voltage on its DC terminals, $U_{\mathrm{I_{dc}}}$, and the reactive power injected to the onshore AC network, Q_{I}.

To study the capability of the WT/WF to provide ancillary services to the onshore AC network, the model has been extended to include the OWF active power control based on the controls proposed in [L. Zeni 2015; J. N. Sakamuri et al. 2017] for OWFs connected to HVDC via VSCs.

For the onshore frequency support (FS) studies, the onshore AC network is modelled as a lumped three-phase synchronous generator (SG) with its turbine, governor, exciter and automatic voltage regulator (AVR), and a lumped three-phase load, as depicted in the left side of Figure 2-3. In such system, wind energy represents 25% of the total installed capacity (i.e., the OWF is rated at $400\ \mathrm{MW}$, in a $1600\ \mathrm{MW}$ system). For the onshore power oscillation damping (POD) studies, the onshore AC network is extended to also include—at the HVDC onshore terminal's point of connection with the onshore AC network (PCC)—a connection to an infinite bus through a transmission line, as illustrated in the right side of Figure 2-3. No delays have been considered in the communication of the relevant onshore signals to the OWF.[2]

Figure 2-3: Onshore AC network models for onshore FS (left) and POD (right) studies

[2] Communication delays and more detailed onshore AC network models should be considered, however, when analysing the impact and benefit of the studied services on the onshore synchronous area stability (out of the scope of this document).

PROMOTiON – Progress on Meshed HVDC Offshore Transmission Networks
This project has received funding from the European Union's Horizon 2020 research and innovation programme under grant agreement No 691714.

Switching effects and any delay due to the implementation of the pulse-width modulation (PWM) have been neglected, and ideal average models have been used for the VSCs. Moreover, the PWM has been assumed to be done in the linear range, and the VSC filter dynamics have not been considered. All components have been assumed to be sized/designed considering the overloading capabilities required to provide the studied ancillary services.

2.1. ONSHORE FREQUENCY SUPPORT

A simplified block diagram of the OWF (group) functionality for providing onshore FS is presented in Figure 2-4. The onshore frequency, f_{on}, is calculated from the alternating voltage measured at the PCC and is communicated continuously to the OWF (group). The OWF (group) decreases its active power output upon detecting a significant onshore frequency increase. Additional active power is necessary for the OWF (group) to increase its active power output upon detecting an onshore frequency decrease. Such additional power can be made available by preventively operating the OWF (group) constantly curtailed. Moreover, some additional boosting active power can be extracted for a relatively short period of time, from the kinetic energy stored in the rotating masses of the WT rotor and drive train systems, at the expense of the active power output dropping below its pre-boost value afterwards [PROMOTioN 2017; PROMOTioN 2016; G. C. Tarnowski 2011].

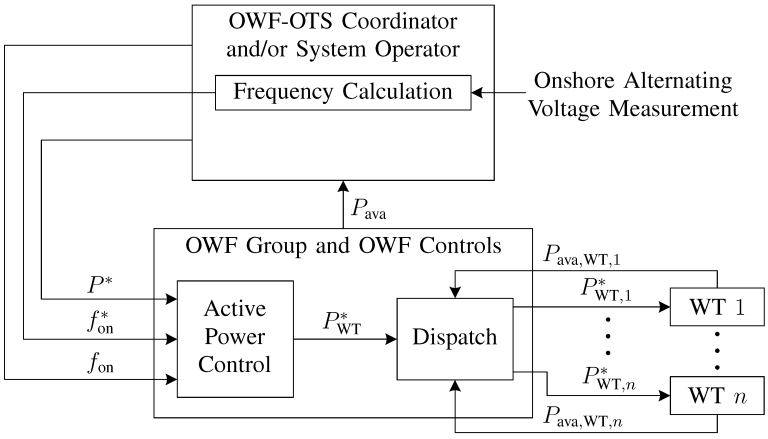

Figure 2-4: Simplified block diagram of the OWF (group) functionality for providing onshore frequency support

Two kinds of frequency response have been considered: primary frequency response (PFR) and fast frequency response (FFR). The PFR is based on an active-power-frequency droop, with the reserves from preventively curtailed operation considered as the source of additional active power during onshore under-frequency events. Based on the rate of change of the frequency deviation, the FFR is meant to contribute to the stabilisation of the onshore AC networks during the first stage of large frequency excursions. The kinetic energy stored in the rotating masses of the WT rotor and drive train systems has been considered as the main source of additional power/energy for such response during onshore underfrequency events [PROMOTioN 2017; L. Zeni 2015; G. C. Tarnowski 2011].

This project has received funding from the European Union's Horizon 2020 research and innovation programme under grant agreement No 691714.

Based on the controls proposed in [L. Zeni 2015; J. N. Sakamuri *et al.* 2017] for OWFs connected to HVDC via VSCs, the OWF (group) active power control model shown in Figure 2-5 is used to study the capability of the WT/WF to provide FS to the onshore AC network. In the right side of Figure 2-5, a PI regulator controls the OWF (group) active power output, P, which is—in the studied system—equal to P_{WT}. A first-order low-pass filter (LPF) is applied to the corresponding measurement signal. Physical and control limits (e.g., those imposed by the WTs) are modelled by means of corresponding restrictions on the regulator's output value and its rate of change. P can be controlled to follow the OWF (group) active power reference, P^*, which is normally equal to or lower than the aerodynamic power available from the wind, $P_{\mathrm{ava}}(v)$, i.e., $\hat{P} = P^* \leq P_{\mathrm{ava}}(v)$.

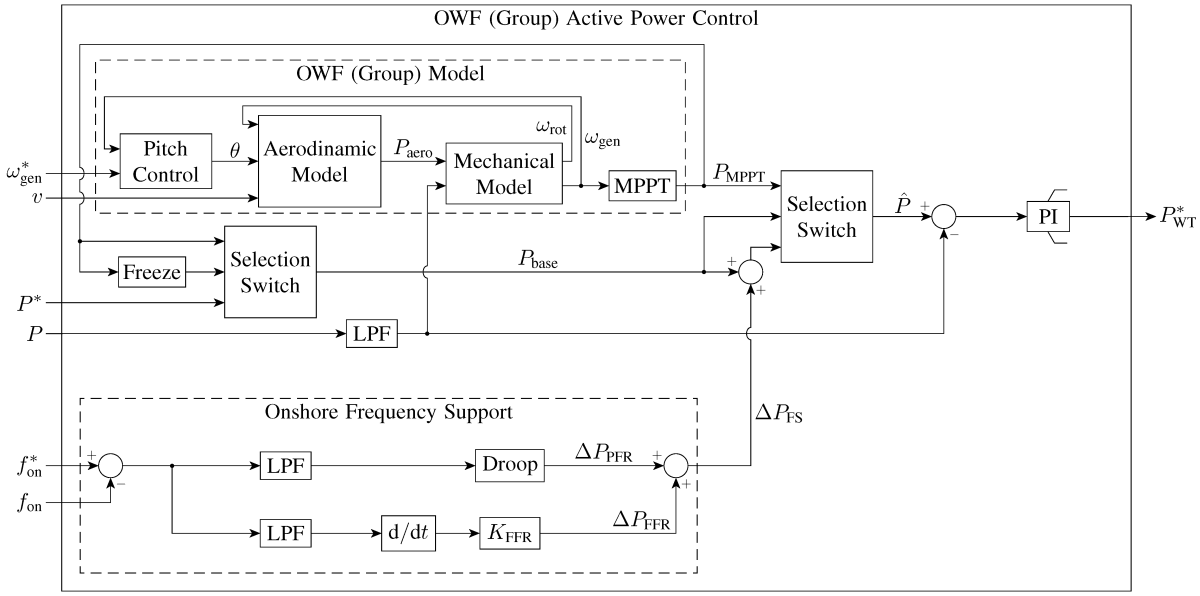

Figure 2-5: OWF (group) active power control model for onshore frequency support studies

An internal aggregated model of the OWF (group), shown in the top-left area of Figure 2-5, is included to represent the WT rotor dynamics relevant to the study of FS from WFs and the overloading of the WTs. It is based on those used in [J. N. Sakamuri et al. 2017; A. D. Hansen et al. 2014; G. Rousi 2013] and consists mainly of an aerodynamic model, a mechanical model, a pitch control model and a maximum power point tracking (MPPT) look-up table.

If the OWF (group) is not required to curtail its production, its WTs follow their normal production characteristic (MPPT curve) i.e., $\hat{P} = P_{\mathrm{MPPT}}(\omega_{\mathrm{gen}})$. While operating on such curve, the WT aerodynamic efficiency is optimal for wind speeds lower than the nominal one, $v < 1\ \mathrm{pu}$, the pitch control is inactive and the WTs operate at a constant zero pitch angle, $\theta = 0$. For higher wind speeds, the WTs run at rated power, and the pitch controller keeps the WT generator rotational speed, ω_{gen}, at its nominal value [A. D. Hansen *et al.* 2014] i.e., $P_{\mathrm{MPPT}}(\omega_{\mathrm{gen}} = 1\ \mathrm{pu}) = 1\ \mathrm{pu}$. When the OWF (group) curtails its production, $\hat{P} = P^* < P_{\mathrm{aero}} = P_{\mathrm{ava}}(v)$, the power imbalance, $P_{\mathrm{aero}} > P$,

This project has received funding from the European Union's Horizon 2020 research and innovation programme under grant agreement No 691714.

causes the WT rotors to accelerate until ω_{gen} reaches $1\,\text{pu}$. To maintain $\omega_{\text{gen}} = 1\,\text{pu}$, the pitch control then increases θ (i.e., pitches the WT blades), which decreases the aerodynamic/mechanical power, P_{aero}, until power balance is restored, $P_{\text{aero}} = P < P_{\text{MPPT}} = 1\,\text{pu}$.

To provide FS to the onshore AC network, the base active power reference, P_{base}, is modified, as shown at the bottom of Figure 2-5, by means of an additional active power reference, ΔP_{FS}, based on the onshore frequency, f_{on}, which is communicated continuously to the WF (group) i.e., $\hat{P} = P_{\text{base}} + \Delta P_{\text{FS}}(f_{\text{on}})$. PFR is implemented by including in ΔP_{FS} a component, ΔP_{PFR}, proportional to the deviation of f_{on} from its nominal/reference value, $f_{\text{on}}^{*} = 1\,\text{pu}$, calculated using a (piecewise-defined) frequency-active-power droop characteristic based on the one shown in Figure 2-6. Moreover, a component, ΔP_{FFR}, proportional to the rate of change of such deviation, $\mathrm{d}f_{\text{on}}/\mathrm{d}t$, is added to provide FFR.

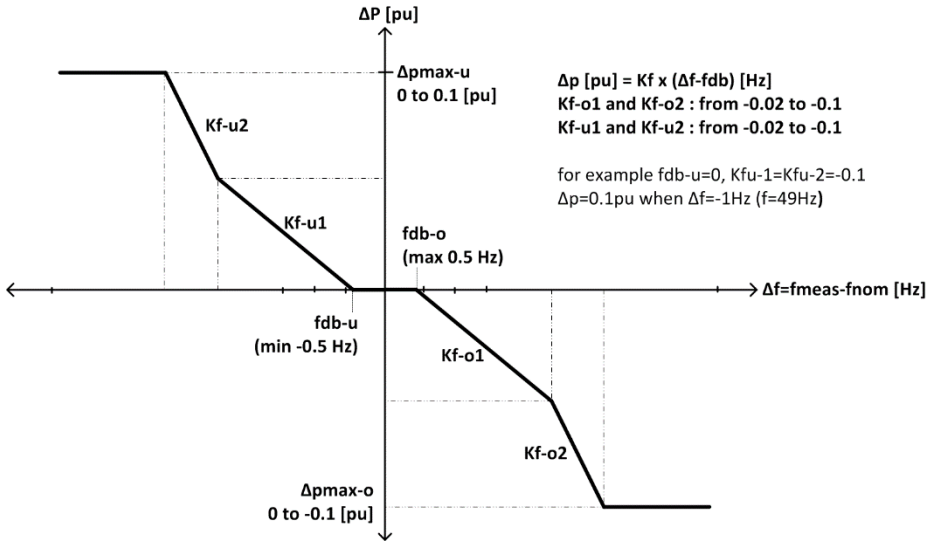

Figure 2-6: OWF PFR capability to onshore frequency changes (droop) [PROMOTioN 2016]

In order to extract kinetic energy from their rotating masses, WTs are overloaded when providing FFR during onshore under-frequency events. During overloading, $\hat{P} = P_{\text{base}} + \Delta P_{\text{FS}} > P_{\text{aero}} \leq P_{\text{ava}}(v)$, the power imbalance, $P_{\text{aero}} < P$, causes the WT rotors to decelerate (ω_{gen} decreases), which results in P_{MPPT} also decreasing. After releasing the overloading, the WTs are allowed to recover their speed by operating on the MPPT curve, $\hat{P} = P_{\text{MPPT}} \leq P_{\text{aero}}$, until $P = P_{\text{aero}} = P^{*} + \Delta P_{\text{FS}}$.

Three WT overloading methods have been considered, based on three different approaches to setting P_{base} during overloading (inputs to the selection switch in the left side of Figure 2-5), as illustrated in Figure 2-7. In the External MPPT Method, P_{base} is fixed at the (frozen) value of P_{MPPT} just before the start of the overloading, $P_{\text{base}} = P_{\text{MPPT}_0}$. In the Internal Method, the WT dynamics are considered during overloading by having $P_{\text{base}} = P_{\text{MPPT}}$, resulting in a smaller decrease in P and a faster recovery (shorter recovery period, T_{rec}) after releasing the overloading [J. N. Sakamuri *et al.* 2017; S. Wachtel and A. Beekmann 2009]. In the External Reference Method, P_{base} is set externally, $P_{\text{base}} = P^{*}$, and can thus be set to e.g., a constant value of less than $P_{\text{MPPT}_0} = 1\,\text{pu}$ in the case of preventively curtailed production [O. Saborío-Romano *et al.* 2017].

This project has received funding from the European Union's Horizon 2020 research and innovation programme under grant agreement No 691714.

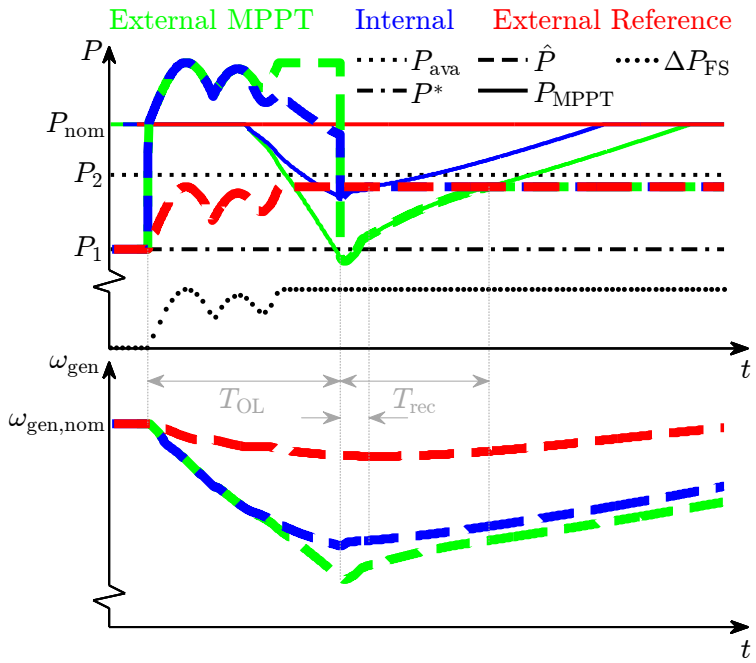

Figure 2-7: Wind turbine overloading methods; $\hat{P} = P_{\text{base}} + \Delta P_{\text{FS}}$

2.2. ONSHORE POWER OSCILLATION DAMPING

A simplified block diagram of the OWF (group) functionality for providing onshore POD is shown in Figure 2-8. The power through the transmission line onshore, P_{on}, is calculated from the alternating voltage and current measured at the PCC and is monitored by the OWF-OTS coordinator and/or the system operator. When onshore power oscillations are detected, a corresponding signal, ΔP_{on}, is generated and sent to the OWF (group), together with the activation of a flag, F_{POD}, which switches the OWF (group) controller to the POD control mode. In such mode, the OWF (group) modulates its active power output so as to produce damping torque: an electrical torque component in phase with the SG's speed deviation, $\Delta\omega_{\text{SG}}$, increasing the decay rate of the oscillations as a result [PROMOTioN 2017; PROMOTioN 2016; L. Zeni 2015].

This project has received funding from the European Union's Horizon 2020 research and innovation programme under grant agreement No 691714.

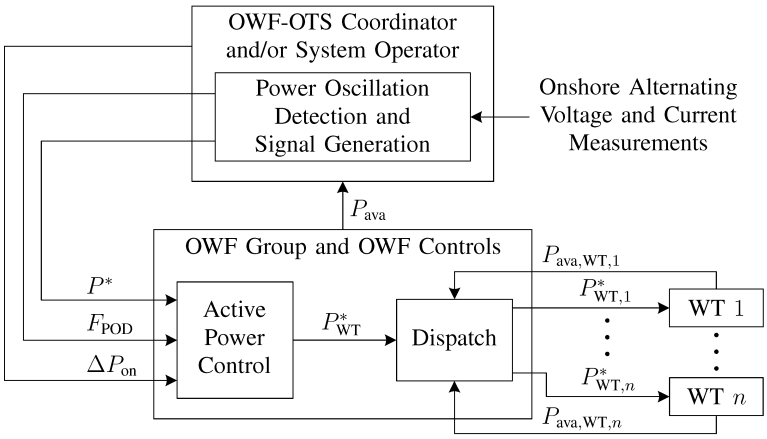

Figure 2-8: Simplified block diagram of the OWF (group) functionality for providing onshore power oscillation damping

Based on the controls proposed in [L. Zeni 2015] for OWFs connected to HVDC via VSCs, the OWF (group) active power control model shown in Figure 2-9 is used to study the capability of the WT/WF to provide onshore POD. The PI regulator and LPF correspond to those in Figure 2-5. Following the activation of F_{POD}, the controller switches to POD control mode: the PI regulator's output (control) signal is frozen and an additional oscillatory damping active power reference, ΔP_{POD}, is superimposed, based on the onshore power oscillation signal, ΔP_{on}, sent to the OWF (group), $P^*_{\mathrm{WT}} = P^*_{\mathrm{WT_0}} + \Delta P_{\mathrm{POD}}(\Delta P_{\mathrm{on}})$. The corresponding lead compensator provides the necessary phase shift (around 90°) to align ΔP_{POD} with $\Delta\omega_{\mathrm{SG}}$ (and thus with the damping torque). Since ΔP_{POD} does not entail an additional net energy delivery to the onshore AC network, no preventively curtailed operation has been considered in the corresponding studies. The WTs are thus briefly overloaded (with the External Reference Method) during the positive semi-period of ΔP_{POD} and recover their speed during its negative semi-period [L. Zeni 2015; S. Goumalatsos 2014].

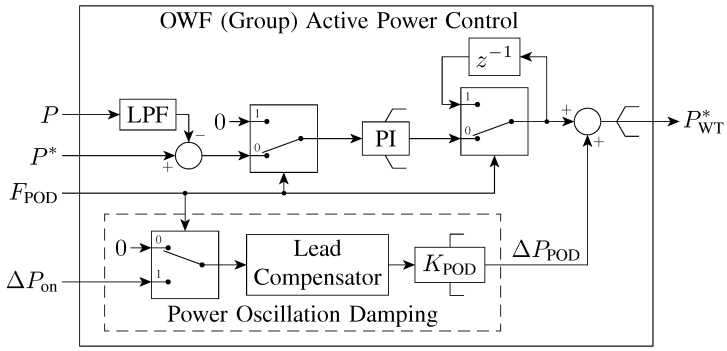

Figure 2-9: OWF (group) active power control model for onshore power oscillation damping studies

Since the restrictions on the PI regulator's output (control) signal are also bypassed, the same restrictions are imposed on the value of P^*_{WT}. In POD control mode, however, the restrictions on its rate of change, $\mathrm{d}P^*_{\mathrm{WT}}/\mathrm{d}t$, are considered to be less stringent than those usually imposed by the WTs, which may be necessary if POD is to be provided with a certain minimum performance [L. Zeni 2015].

This project has received funding from the European Union's Horizon 2020 research and innovation programme under grant agreement No 691714.

3. SIMULATION RESULTS

Results of the performed electromagnetic transient (EMT) simulations are presented in this chapter. The simulation cases are summarised in Table 3-1. Each figure presents results of a simulation case, including a base subcase response corresponding to no provision of ancillary services from the OWF to the onshore AC network. The OWF active power reference, P^*, the wind speed, v, and thus the (total) available aerodynamic power, $P_{\text{ava}}(v)$, have been considered constant throughout each simulation case.

Table 3-1: Simulation cases

Case	Onshore Event	Production	Wind	$P_{\text{ava}}(v)$	P^*	Figure
1	Over-frequency	Normal	Low	0.1 pu	0.1 pu	Figure 3-1
2	Over-frequency	Curtailed	Low	0.2 pu	0.1 pu	Figure 3-2
3	Over-frequency	Normal	Medium	0.5 pu	0.5 pu	Figure 3-3
4	Over-frequency	Curtailed	Medium	0.6 pu	0.5 pu	Figure 3-4
5	Over-frequency	Normal	High	1 pu	1 pu	Figure 3-5
6	Over-frequency	Curtailed	High	1 pu	0.9 pu	Figure 3-6
7	Under-frequency	Normal	Low	0.1 pu	0.1 pu	Figure 3-7
8	Under-frequency	Normal	Medium	0.5 pu	0.5 pu	Figure 3-8
9	Under-frequency	Normal	High	1 pu	1 pu	Figure 3-9
10	Under-frequency	Curtailed	Low	0.2 pu	0.1 pu	Figure 3-10
11	Under-frequency	Curtailed	Medium	0.6 pu	0.5 pu	Figure 3-11
12	Under-frequency	Curtailed	High	1 pu	0.9 pu	Figure 3-12
13	Power Oscillation	Normal	Low	0.1 pu	0.1 pu	Figure 3-13
14	Power Oscillation	Normal	Medium	0.5 pu	0.5 pu	Figure 3-14
15	Power Oscillation	Normal	High	1 pu	1 pu	Figure 3-15

3.1. ONSHORE FREQUENCY SUPPORT

Frequency events are simulated by means of 15% load step changes (i.e., $\pm 240\ \text{MW}/1600\ \text{MW}$) at $t = 0.5\ \text{s}$. Each figure includes a base subcase response, corresponding to no FS from the OWF to the onshore AC network (i.e., the frequency response consisting solely of that of the lumped SG onshore), and relevant simulation subcases. The simulation subcases are summarised in Table 3-2. As can be seen in all figures, the frequency response can be improved by having the OWF modulate P in response to an onshore frequency event.

This project has received funding from the European Union's Horizon 2020 research and innovation programme under grant agreement No 691714.

Table 3-2: Frequency support simulation subcases

Sub-case	Prod.	PFR	FFR	WT Overloading ($0.5s < t < 13s$)	$\hat{P}(t)$ $0.5\text{s} < t < 13\text{s}$	$\hat{P}(t)$ $t \geq 13\text{s}$
CBase	Curtailed	No	No	No	$P^*(t)$	
CF	Curtailed	No	Yes	No	$P^*(t) + \Delta P_{\text{FFR}}(t) \equiv \hat{P}_{\text{A}}(t)$	
CP	Curtailed	Yes	No	No	$P^*(t) + \Delta P_{\text{PFR}}(t)$	
CPF	Curtailed	Yes	Yes	No	$\hat{P}_{\text{A}}(t) + \Delta P_{\text{PFR}} \equiv P^*(t) + \Delta P_{\text{FS}}(t) \equiv \hat{P}_{\text{B}}(t)$	
CPFE-MPPT	Curtailed	Yes	Yes	External MPPT Method	$P_{\text{MPPT}}(0.5\text{s}) + \Delta P_{\text{FS}}(t)$	$\min\{P_{\text{MPPT}}(t), \hat{P}_{\text{B}}(t)\}$
CPFE-Ref	Curtailed	Yes	Yes	External Reference Method	$\hat{P}_{\text{B}}(t)$	$\min\{P_{\text{MPPT}}(t), \hat{P}_{\text{B}}(t)\}$
CPFI	Curtailed	Yes	Yes	Internal Method	$P_{\text{MPPT}}(t) + \Delta P_{\text{FS}}(t)$	$\min\{P_{\text{MPPT}}(t), \hat{P}_{\text{B}}(t)\}$
NBase	Normal	No	No	No	$P^*(t)$	
NF	Normal	No	Yes	No	$P^*(t) + \Delta P_{\text{FFR}}(t)$	
NFE-MPPT	Normal	No	Yes	External MPPT Method	$P_{\text{MPPT}}(0.5\text{s}) + \Delta P_{\text{FFR}}(t)$	$\min\{P_{\text{MPPT}}(t), \hat{P}_{\text{A}}(t)\}$
NFI	Normal	No	Yes	Internal Method	$P_{\text{MPPT}}(t) + \Delta P_{\text{FFR}}(t)$	$\min\{P_{\text{MPPT}}(t), \hat{P}_{\text{A}}(t)\}$
NP	Normal	Yes	No	No	$P^*(t) + \Delta P_{\text{PFR}}(t)$	
NPF	Normal	Yes	Yes	No	$\hat{P}_{\text{B}}(t)$	
NPFE-MPPT	Normal	Yes	Yes	External MPPT Method	$P_{\text{MPPT}}(0.5\text{s}) + \Delta P_{\text{FS}}(t)$	$\min\{P_{\text{MPPT}}(t), \hat{P}_{\text{B}}(t)\}$

3.1.1 ONSHORE OVER-FREQUENCY EVENT

The OWF's response to an onshore over-frequency event is shown in Figure 3-2 and Figure 3-1 for low wind speed, Figure 3-4 and Figure 3-3 for medium wind speed, and Figure 3-6 and Figure 3-5 for high wind speed. Figure 3-2, Figure 3-4 and Figure 3-6 correspond to the initial condition of normal (maximum) OWF production, $P_0 = P_0^* = P_{\text{ava}} = P_{\text{MPPT}_0}$. Figure 3-1, Figure 3-3 and Figure 3-5 correspond to the initial condition of preventively curtailed OWF production to provide active power reserves of 10%, $P_0 = P_0^* = P_{\text{ava}} - 0.1\text{ pu} \Rightarrow \omega_{\text{gen}_0} = 1\text{ pu} = P_{\text{MPPT}_0}$. The grey and red signals in each figure represent the base subcase, $\text{NBase}/\text{CBase}$, and the subcase with the OWF providing PFR only, NP/CP, respectively. The orange curves in each figure represent the subcase with the OWF providing FFR only, NF/CF, while the black signals represent the provision of both PFR and FFR, NPF/CPF. In providing onshore FS, the OWF reduces P in response to the onshore over-frequency event. Since no additional power is needed, the WTs are not overloaded.

The OWF's PFR reduces f_{on} and maintains it at a lower value, as depicted in NP/CP, also reducing the frequency zenith as a consequence. However, the decrease in P at low wind speed is restricted by the minimum production

This project has received funding from the European Union's Horizon 2020 research and innovation programme under grant agreement No 691714.

limit, $P \leq 2.5\%$, imposed by the non-linear properties of the DR [PROMOTioN 2017], as shown in Figure 3-2 and Figure 3-1. The power imbalance, $P_{\text{aero}} > P$, causes the WT rotors to accelerate until ω_{gen} reaches $1\ \text{pu}$. To maintain $\omega_{\text{gen}} = 1\ \text{pu}$, the pitch control then increases θ (i.e., pitches the WT blades), which decreases P_{aero}, until power balance is restored, $P_{\text{aero}} = P < P_{\text{MPPT}} = 1\ \text{pu}$.

The FFR reduces the rate of change of frequency (ROCOF) just after the event, also reducing the frequency zenith as a consequence, as illustrated in NF/CF. Nevertheless, the constraints imposed on the rate of change of the WT active power references, $-0.1\ \text{pu} \leq \text{d}P^*_{\text{WT}}/\text{d}t \leq 0.1\ \text{pu}$, limit the speed of such response and thus the corresponding improvement in the onshore FS. To further improve the frequency response, both PFR and FFR can be combined, and the restriction $\text{d}P^*_{\text{WT}}/\text{d}t \leq 0$ can be briefly applied following the frequency zenith, on which $\text{d}f_{\text{on}}/\text{d}t$ changes sign, as depicted in NPF/CPF.

This project has received funding from the European Union's Horizon 2020 research and innovation programme under grant agreement No 691714.

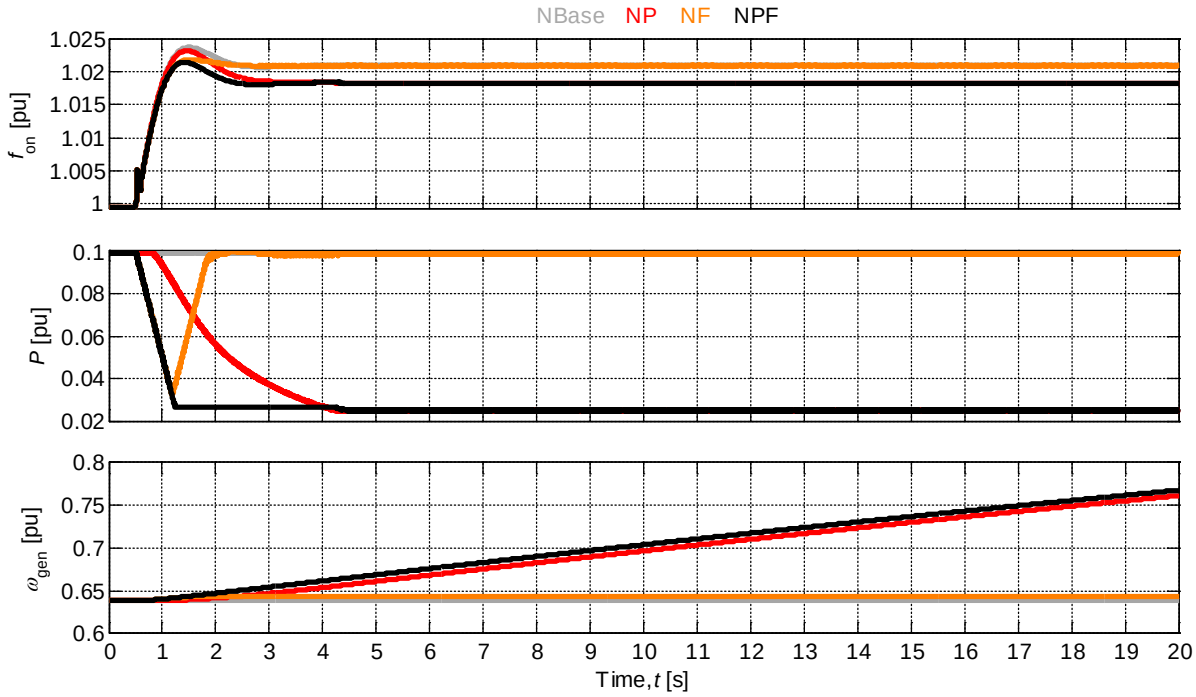

Figure 3-1: Case 1 – OWF's response to an onshore over-frequency event ($t = 0.5s$) at low wind speed – No Reserves – NBase: $\hat{P} = P^*$, NP: $\hat{P} = P^* + \Delta P_{\mathrm{PFR}}$, NF: $\hat{P} = P^* + \Delta P_{\mathrm{FFR}}$, NPF: $\hat{P} = P^* + \Delta P_{\mathrm{PFR}} + \Delta P_{\mathrm{FFR}}$

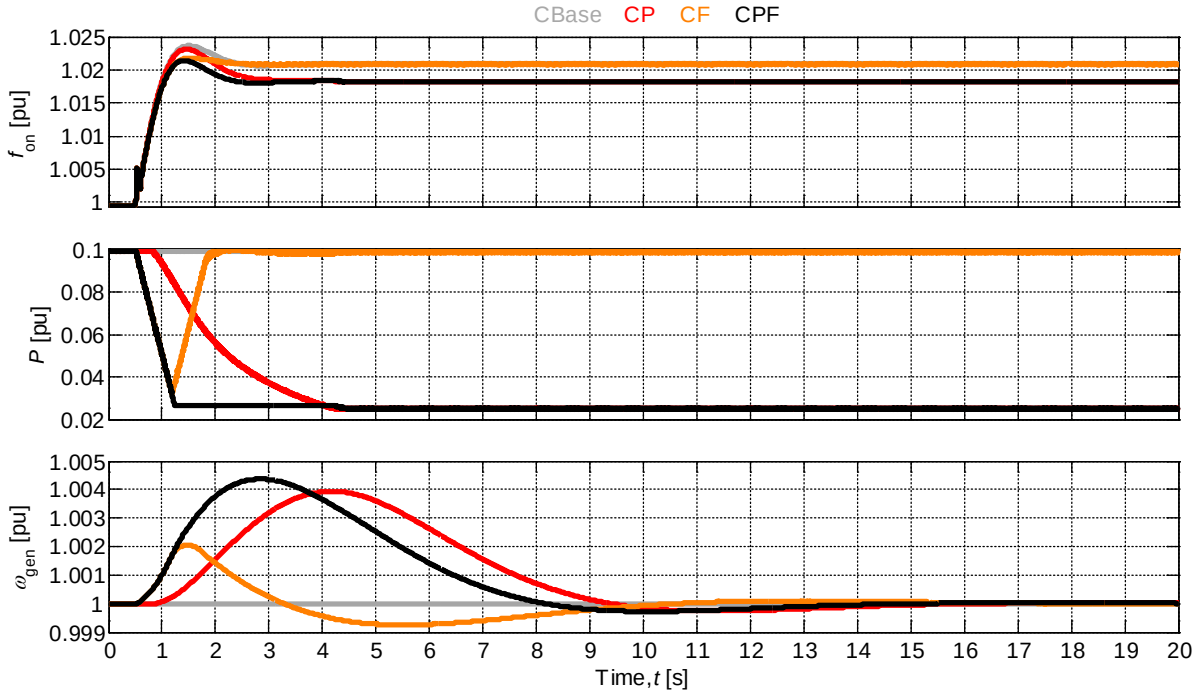

Figure 3-2: Case 2 – OWF's response to an onshore over-frequency event ($t = 0.5s$) at low wind speed – Reserves: 10% – CBase: $\hat{P} = P^*$, CP: $\hat{P} = P^* + \Delta P_{\mathrm{PFR}}$, CF: $\hat{P} = P^* + \Delta P_{\mathrm{FFR}}$, CPF: $\hat{P} = P^* + \Delta P_{\mathrm{PFR}} + \Delta P_{\mathrm{FFR}}$

PROMOTiON – Progress on Meshed HVDC Offshore Transmission Networks

This project has received funding from the European Union's Horizon 2020 research and innovation programme under grant agreement No 691714.

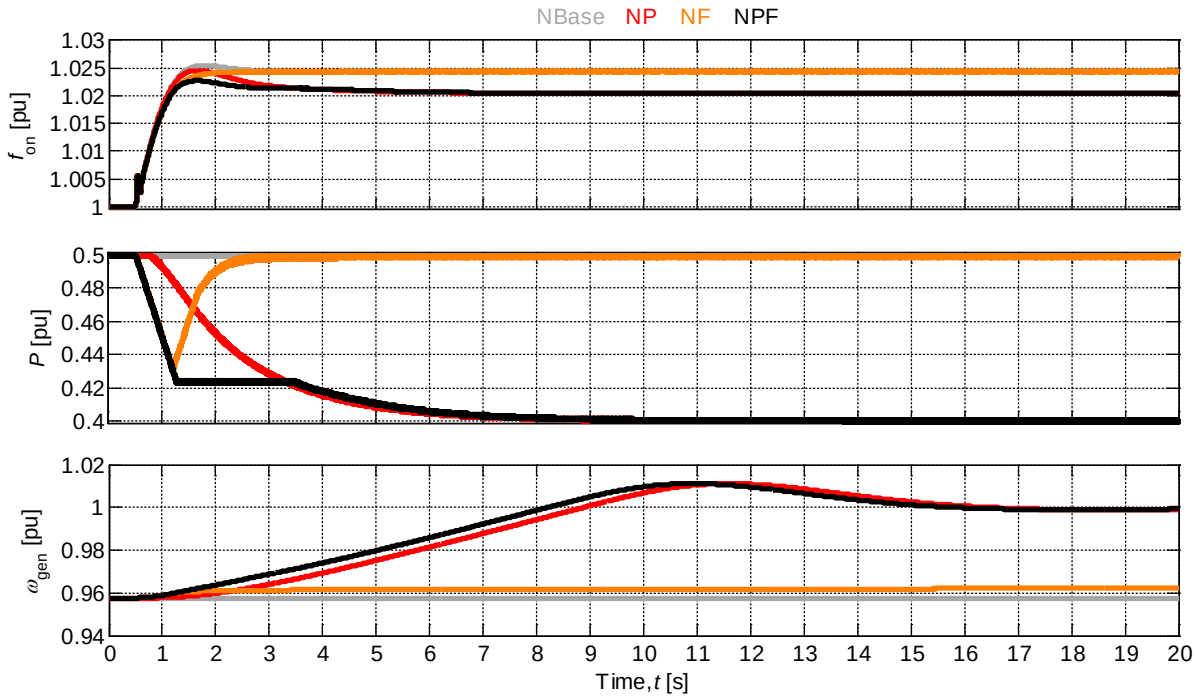

Figure 3-3: Case 3 – OWF's response to an onshore over-frequency event ($t = 0.5$s) at medium wind speed – No Reserves – NBase: $\hat{P} = P^*$, NP: $\hat{P} = P^* + \Delta P_{\text{PFR}}$, NF: $\hat{P} = P^* + \Delta P_{\text{FFR}}$, NPF: $\hat{P} = P^* + \Delta P_{\text{PFR}} + \Delta P_{\text{FFR}}$

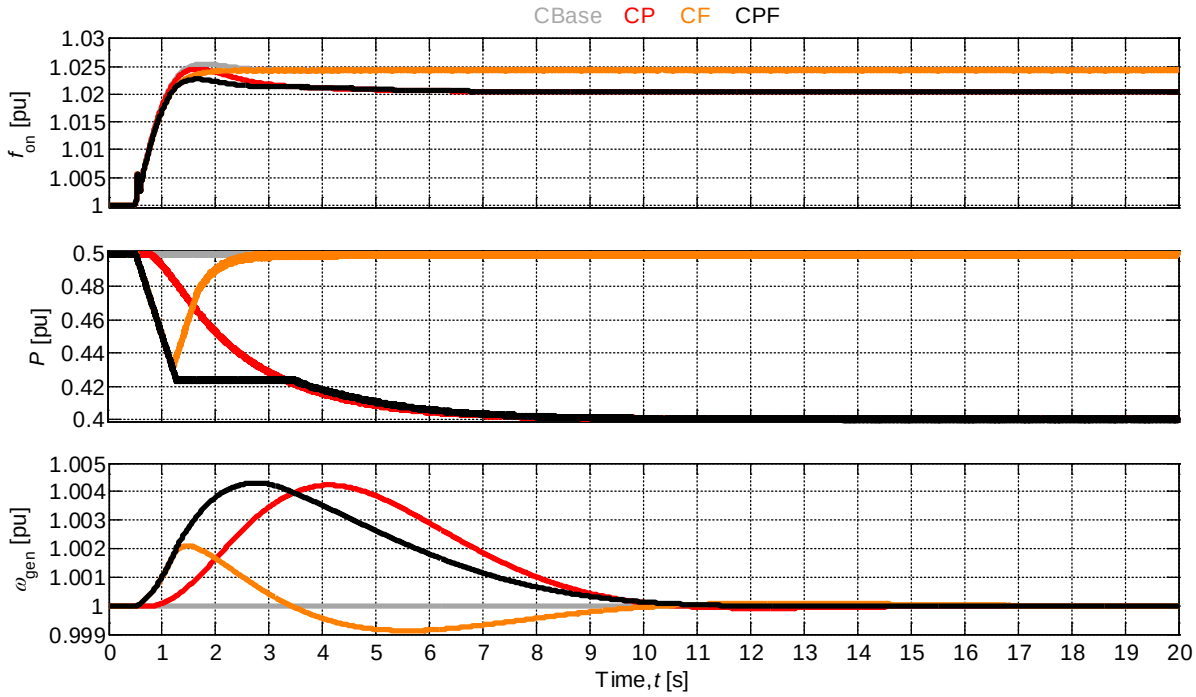

Figure 3-4: Case 4 – OWF's response to an onshore over-frequency event ($t = 0.5$s) at medium wind speed – Reserves: 10% – CBase: $\hat{P} = P^*$, CP: $\hat{P} = P^* + \Delta P_{\text{PFR}}$, CF: $\hat{P} = P^* + \Delta P_{\text{FFR}}$, CPF: $\hat{P} = P^* + \Delta P_{\text{PFR}} + \Delta P_{\text{FFR}}$

PROMOTiON – Progress on Meshed HVDC Offshore Transmission Networks

This project has received funding from the European Union's Horizon 2020 research and innovation programme under grant agreement No 691714.

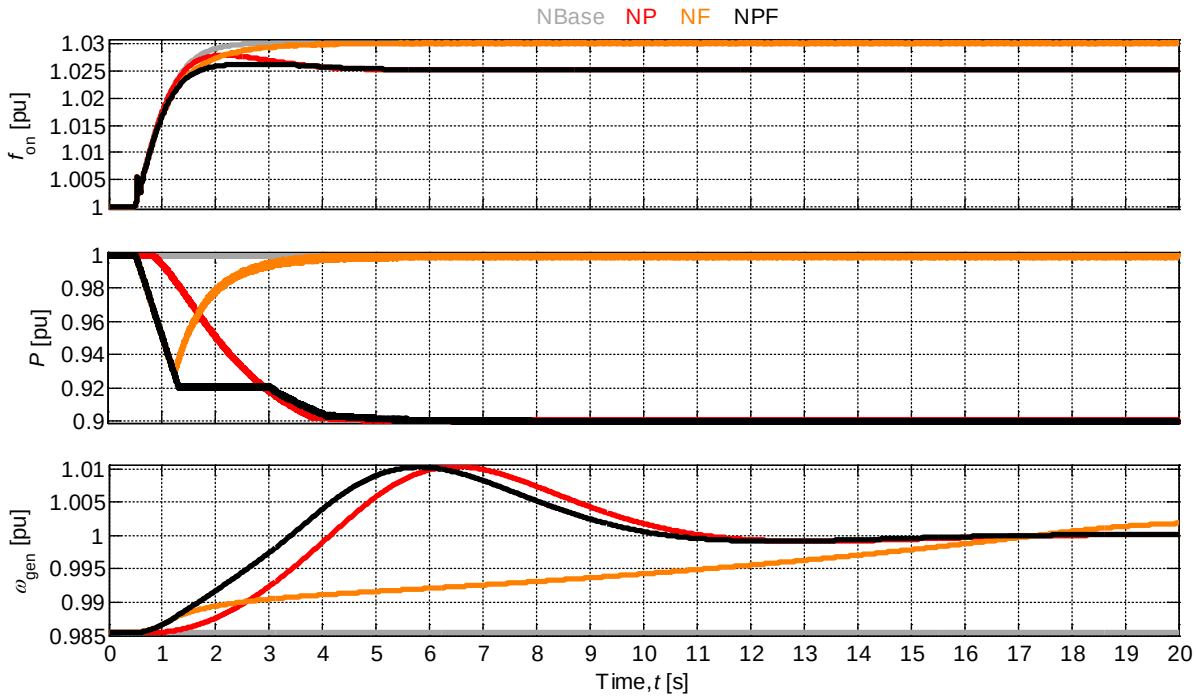

Figure 3-5: Case 5 – OWF's response to an onshore over-frequency event ($t = 0.5s$) at high wind speed – No Reserves – NBase: $\hat{P} = P^*$, NP: $\hat{P} = P^* + \Delta P_{\text{PFR}}$, NF: $\hat{P} = P^* + \Delta P_{\text{FFR}}$, NPF: $\hat{P} = P^* + \Delta P_{\text{PFR}} + \Delta P_{\text{FFR}}$

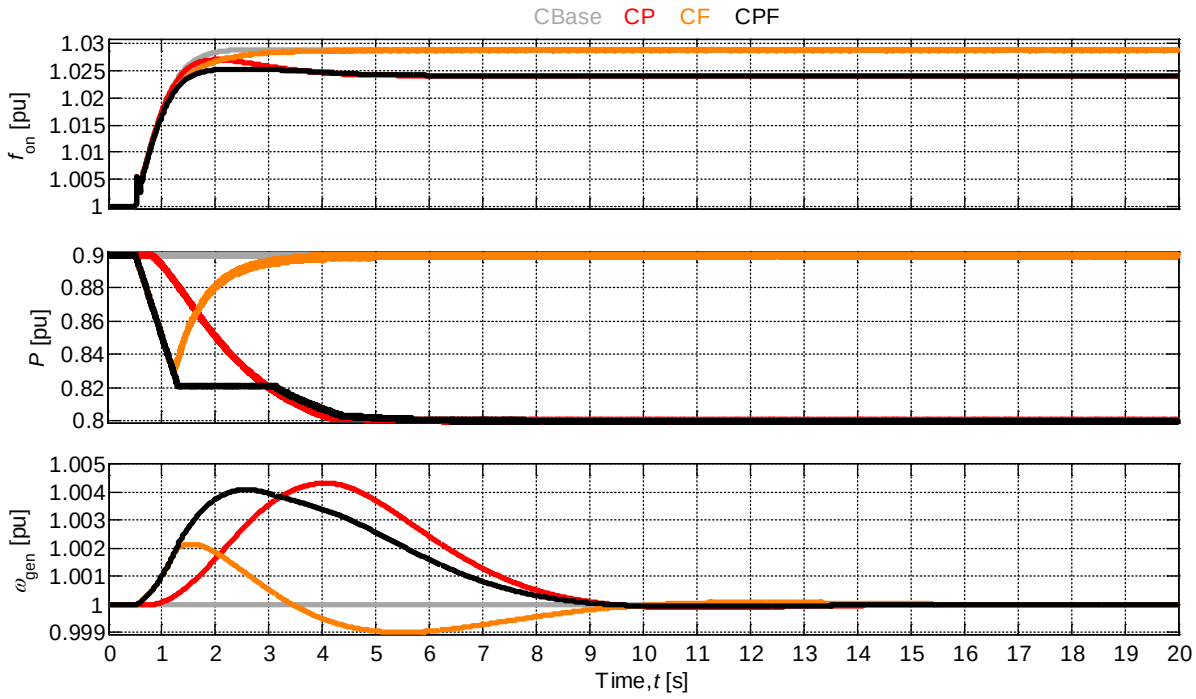

Figure 3-6: Case 6 – OWF's response to an onshore over-frequency event ($t = 0.5s$) at high wind speed – Reserves: 10% – CBase: $\hat{P} = P^*$, CP: $\hat{P} = P^* + \Delta P_{\text{PFR}}$, CF: $\hat{P} = P^* + \Delta P_{\text{FFR}}$, CPF: $\hat{P} = P^* + \Delta P_{\text{PFR}} + \Delta P_{\text{FFR}}$

This project has received funding from the European Union's Horizon 2020 research and innovation programme under grant agreement No 691714.

3.1.2 ONSHORE UNDER-FREQUENCY EVENT

In providing onshore FS, the OWF increases P in response to the onshore under-frequency event, for which additional active power is necessary. Such additional power can be made available by preventively operating the OWF constantly curtailed. Moreover, some additional boosting active power can be extracted for a relatively short period of time, from the kinetic energy stored in the rotating masses of the WT rotor and drive train systems, at the expense of the active power output dropping below its pre-boost value afterwards. In all cases with WT overloading, the overloading is released at $t = 13\,s$. The corresponding simulation results are presented and discussed in Section 3.1.2.1 and Section 3.1.2.2, for normal and preventively curtailed production, respectively.

3.1.2.1 NORMAL PRODUCTION

The OWF's response to an onshore under-frequency event is illustrated in Figure 3-8, Figure 3-8 and Figure 3-9, for low, medium and high wind speeds, respectively, with the initial condition of normal (maximum) OWF production, $P_0 = P_0^* = P_{\text{ava}} = P_{\text{MPPT}_0}$. Since no other source of additional power is considered, the WTs are overloaded whenever the OWF proves onshore FS. The grey curves in each figure correspond to the base subcase, NBase, while the signals in magenta and brown represent the subcases with the OWF providing FFR only, by overloading the WTs with a different method in each subcase. The External MPPT Method is used in the subcase represented by the curves in magenta, NFE-MPPT, whereas the brown signals correspond to the subcase in which the Internal Method is applied, NFI. The green curves in each figure depict the provision of both PFR and FFR, overloading the WTs with the External MPPT Method, NPFE-MPPT.

The OWF can provide FFR by overloading the WTs (at the expense of a reduction in ω_{gen}), reducing the ROCOF just after the event and the frequency nadir as a consequence, as illustrated in NFE-MPPT. However, the speed of such response and corresponding improvement in the onshore FS is limited by the restrictions imposed on $\mathrm{d}P_{\text{WT}}^*/\mathrm{d}t$. When the overloading is released, P and f_{on} are reduced as the WTs recover their speed, producing a new under-frequency event with a nadir that can be greater than the original one in NBase, as shown in Figure 3-8 and Figure 3-9. Moreover, the constraints imposed on $\mathrm{d}P_{\text{WT}}^*/\mathrm{d}t$ worsen the new event by extending its duration. If, however, the Internal Method is used for overloading the WTs, as in NFI, P follows the reduction in $P_{\text{MPPT}}(\omega_{\text{gen}})$, allowing the WTs to fully recover their speed and thus results in no drop in P or f_{on} when the overloading is released.

As illustrated in NPFE-MPPT, PFR can be added to the FS and the constraint $\mathrm{d}P_{\text{WT}}^*/\mathrm{d}t \geq 0$ can be briefly applied following the frequency nadir (on which $\mathrm{d}f_{\text{on}}/\mathrm{d}t$ changes sign) to further improve the frequency response during the overloading period. Such subcase also illustrates the capability of having an overproduction of at least 5% for more than $10\,\text{s}$, until the overloading is released. As a consequence, f_{on} is increased and maintained at a value higher than in the other subcases, at the expense of producing a new onshore under-frequency event with a nadir that can be much greater than the original one in NBase. This also shows that the kinetic energy stored in the rotating masses of WTs is not sufficient for providing PFR.

This project has received funding from the European Union's Horizon 2020 research and innovation programme under grant agreement No 691714.

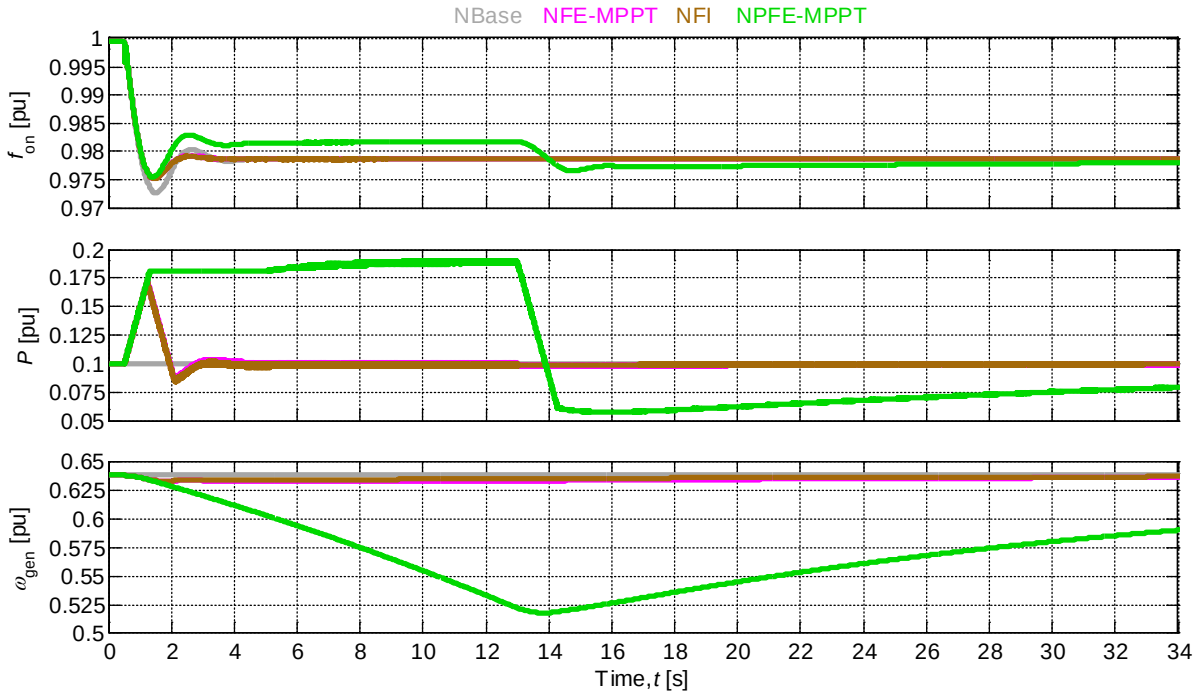

Figure 3-7: Case 7 – OWF's response to an onshore under-frequency event ($t = 0.5s$) at low wind speed – Overloading released at $t = 13s$ – No Reserves – NBase: $\hat{P} = P^*$, NFE-MPPT: $\hat{P} = P_{\mathrm{MPPT_0}} + \Delta P_{\mathrm{FFR}}$, NFI: $\hat{P} = P_{\mathrm{MPPT}} + \Delta P_{\mathrm{FFR}}$, NPFE-MPPT: $\hat{P} = P_{\mathrm{MPPT_0}} + \Delta P_{\mathrm{PFR}} + \Delta P_{\mathrm{FFR}}$

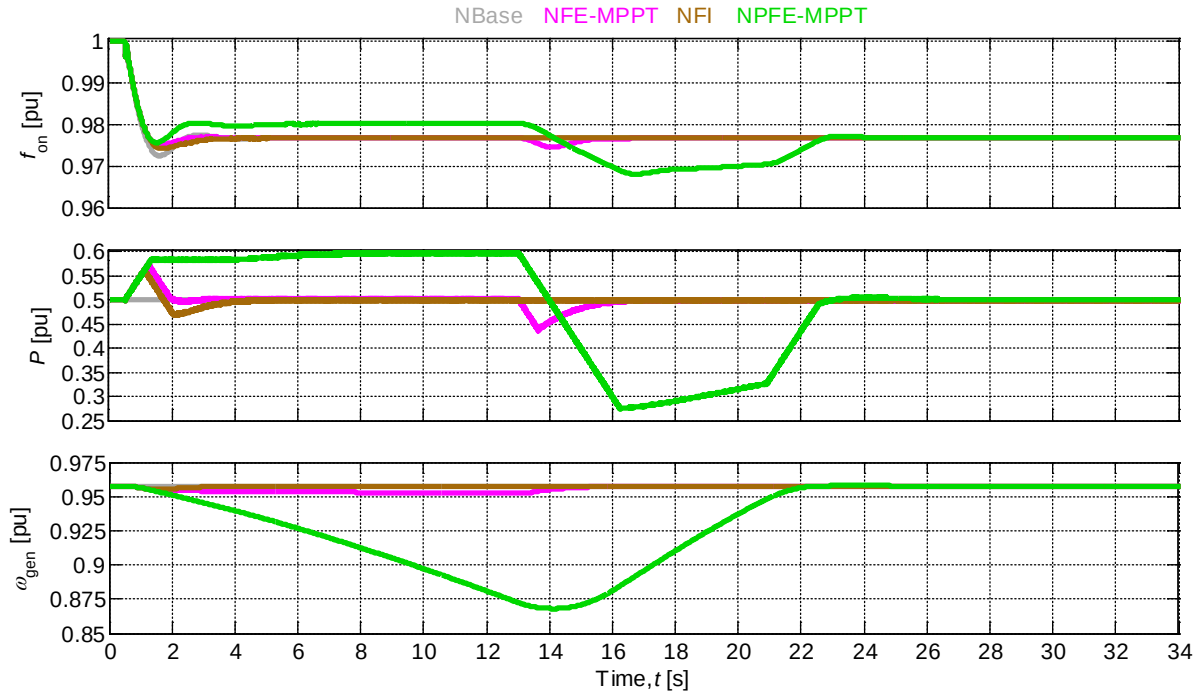

Figure 3-8: Case 8 – OWF's response to an onshore under-frequency event ($t = 0.5s$) at medium wind speed – No Reserves – Overloading released at $t = 13s$ – NBase: $\hat{P} = P^*$, NFE-MPPT: $\hat{P} = P_{\mathrm{MPPT_0}} + \Delta P_{\mathrm{FFR}}$, NFI: $\hat{P} = P_{\mathrm{MPPT}} + \Delta P_{\mathrm{FFR}}$, NPFE-MPPT: $\hat{P} = P_{\mathrm{MPPT_0}} + \Delta P_{\mathrm{PFR}} + \Delta P_{\mathrm{FFR}}$

This project has received funding from the European Union's Horizon 2020 research and innovation programme under grant agreement No 691714.

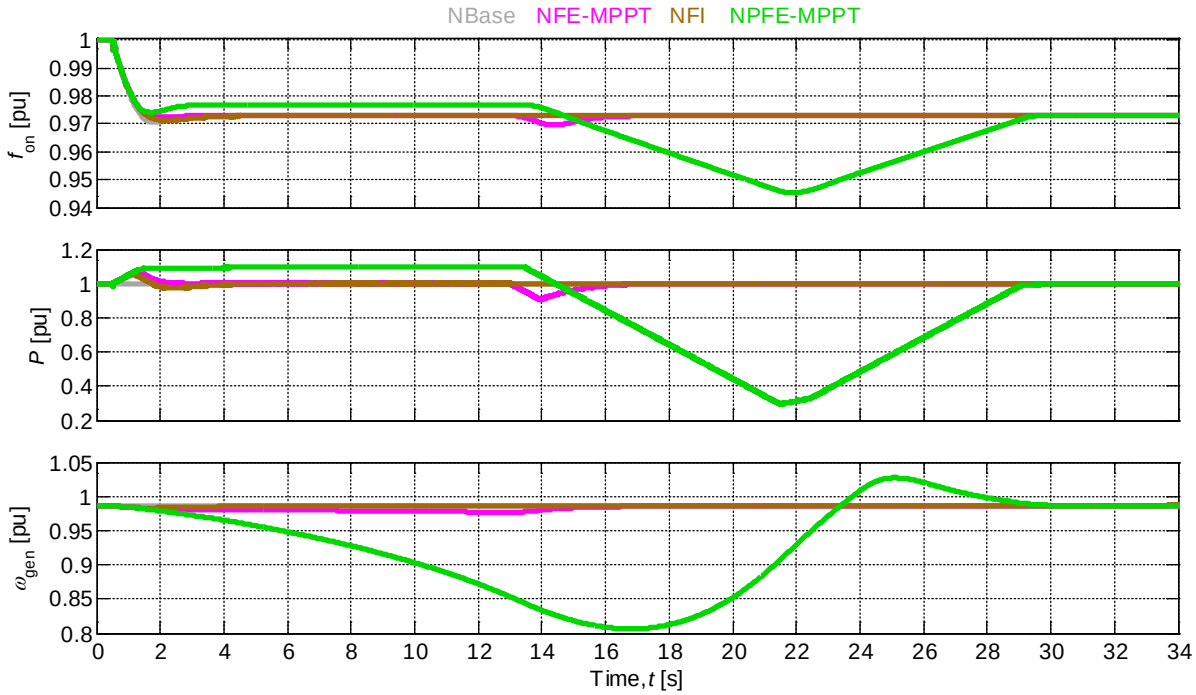

Figure 3-9: Case 9 – OWF's response to an onshore under-frequency event ($t = 0.5s$) at high wind speed – No Reserves – Overloading released at $t = 13s$ – NBase: $\hat{P} = P^*$, NFE-MPPT: $\hat{P} = P_{\mathrm{MPPT_0}} + \Delta P_{\mathrm{FFR}}$, NFI: $\hat{P} = P_{\mathrm{MPPT}} + \Delta P_{\mathrm{FFR}}$, NPFE-MPPT: $\hat{P} = P_{\mathrm{MPPT_0}} + \Delta P_{\mathrm{PFR}} + \Delta P_{\mathrm{FFR}}$

3.1.2.2 CURTAILED PRODUCTION

Figure 3-10, Figure 3-12and Figure 3-11 depict the OWF's response to an onshore under-frequency event at low, medium and high wind speeds, respectively, with the initial condition of preventively curtailed OWF production to provide active power reserves of 10%, $P_0 = P_0^* = P_{\mathrm{ava}} - 0.1\ \mathrm{pu} \Rightarrow \omega_{\mathrm{gen_0}} = 1\ \mathrm{pu} = P_{\mathrm{MPPT_0}}$. The grey and red signals in each figure represent the base subcase, CBase, and the subcase with the OWF providing PFR only, CP, respectively. The orange curves in each figure represent the subcase with the OWF providing FFR only by drawing on the active power reserves i.e., without overloading the WTs, CF. The last sets of signals in each figure depict the provision of both PFR and FFR, overloading the WTs with a different method in each subcase. The External MPPT Method is used in the subcase represented by the green signals (Figure 3-11), $\mathrm{CPFE\text{-}MPPT}$, whereas the blue and yellow curves correspond to the subcases in which the Internal, CPFI, and External Reference, $\mathrm{CPFE\text{-}Ref}$, methods are applied, respectively.

Tapping into the active power reserves, the OWF's PFR increases f_{on} and maintains it at a higher value for as long as the wind allows, as illustrated in CP, also reducing the frequency nadir as a consequence. As depicted in CF, the OWF can also draw on the reserves to provide FFR without overloading the WTs, reducing the ROCOF just after the event and the frequency nadir as a consequence; however, the speed of such response and corresponding reduction of the ROCOF is limited by the restrictions imposed on $\mathrm{d}P_{\mathrm{WT}}^*/\mathrm{d}t$.

PROMOTiON – Progress on Meshed HVDC Offshore Transmission Networks
This project has received funding from the European Union's Horizon 2020 research and innovation programme under grant agreement No 691714.

To further improve the frequency response, both PFR and FFR can be combined, and the constraint $\mathrm{d}P^*_{\mathrm{WT}}/\mathrm{d}t \geq 0$ can be briefly applied following the frequency nadir (on which $\mathrm{d}f_{\mathrm{on}}/\mathrm{d}t$ changes sign), as illustrated in CPFE-Ref. As opposed to CPFE-MPPT and CPFI, the lower value given in this subcase to the base active power reference, $P_{\mathrm{base}} = P^* = P_{\mathrm{ava}} - 0.1\ \mathrm{pu} \leq 0.9\ \mathrm{pu}$, produces no overloading of the WTs i.e., the active power reserves suffice for the provision of both PFR and FFR. If P_{base} is set to a high enough value (e.g., $1\ \mathrm{pu}$), the WTs are overloaded and the OWF produces more than the available aerodynamic power, $P_{\mathrm{ava}}(v)$, at the expense of a reduction in ω_{gen}, as shown in CPFE-MPPT (Figure 3-11) and CPFI. This results in a further reduction of the ROCOF just after the event and thus of the nadir. Such reduction is, however, also limited by the restrictions imposed on $\mathrm{d}P^*_{\mathrm{WT}}/\mathrm{d}t$, making such and any further improvement to the onshore FS smaller. What is more significant: f_{on} is increased and maintained temporarily at a value higher than in CP and CPFE-Ref.

Fixing the value of P_{base} at $P_{\mathrm{MPPT_0}} = 1\ \mathrm{pu}$ in CPFE-MPPT results in an overproduction of at least 5% for about $10\ s$ at high wind speed (Figure 3-11), until the overloading is released. When the overloading is released, P and f_{on} are reduced as the WTs recover their speed, producing a new under-frequency event with a nadir much greater than the original one in CBase. Moreover, the constraints imposed on $\mathrm{d}P^*_{\mathrm{WT}}/\mathrm{d}t$ worsen the new event by extending its duration. If, however, the Internal Method is used for overloading the WTs, as in CPFI, P follows the reduction in $P_{\mathrm{MPPT}}(\omega_{\mathrm{gen}})$ during the overloading, allowing the WTs to start recovering their speed. Such reduction in P during the overproduction period results in a shorter recovery (underproduction) period (after releasing the overloading) with much smaller reductions in P and f_{on}, as illustrated in Figure 3-11.

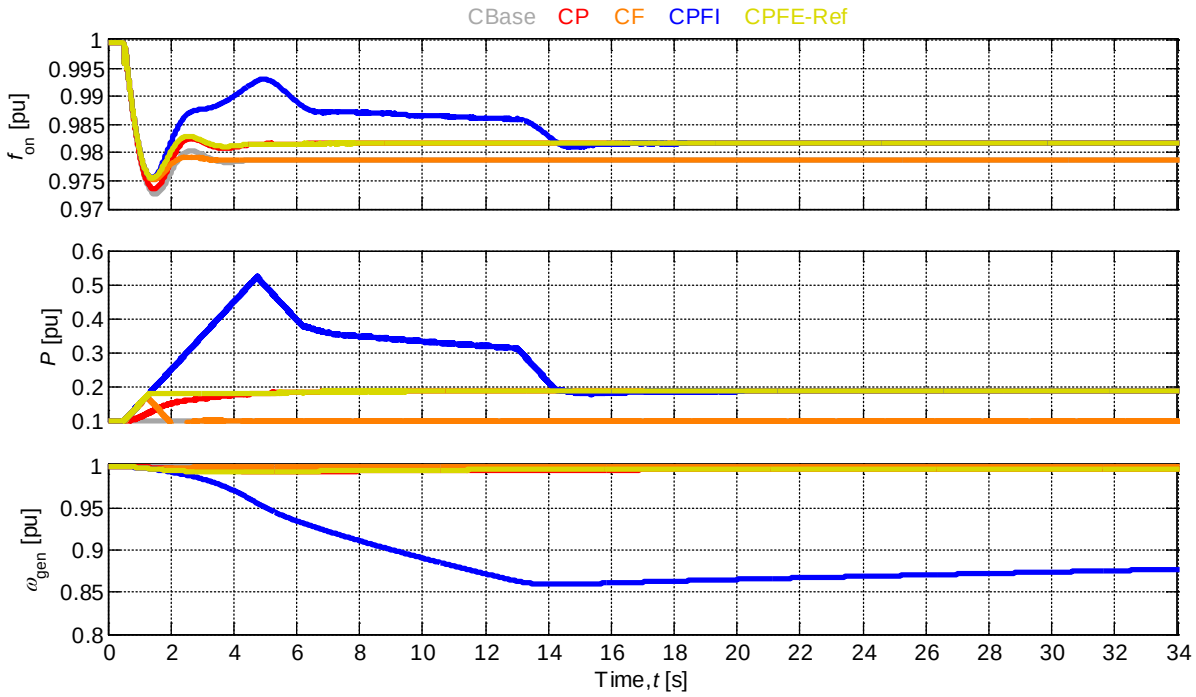

Figure 3-10: Case 10 – OWF's response to an onshore under-frequency event ($t = 0.5s$) at low wind speed – Reserves: 10% – Overloading released at $t = 13s$ – CBase: $\hat{P} = P^*$, CP: $\hat{P} = P^* + \Delta P_{\mathrm{PFR}}$, CF: $\hat{P} = P^* + \Delta P_{\mathrm{FFR}}$, CPFI: $\hat{P} = P_{\mathrm{MPPT}} + \Delta P_{\mathrm{PFR}} + \Delta P_{\mathrm{FFR}}$, CPFE-Ref: $\hat{P} = P^* + \Delta P_{\mathrm{PFR}} + \Delta P_{\mathrm{FFR}}$

This project has received funding from the European Union's Horizon 2020 research and innovation programme under grant agreement No 691714.

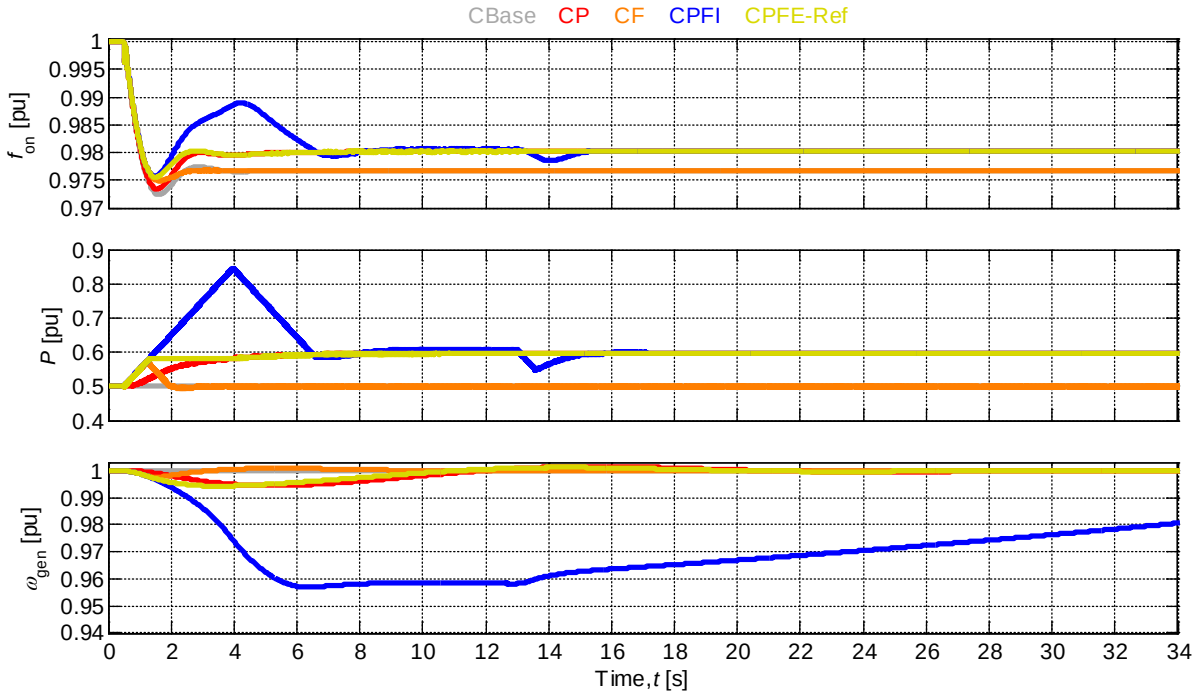

Figure 3-11: Case 11 – OWF's response to an onshore under-frequency event ($t = 0.5s$) at medium wind speed – Reserves: 10% – Overloading released at $t = 13s$ – CBase: $\hat{P} = P^*$, CP: $\hat{P} = P^* + \Delta P_{\mathrm{PFR}}$, CF: $\hat{P} = P^* + \Delta P_{\mathrm{FFR}}$, CPFI: $\hat{P} = P_{\mathrm{MPPT}} + \Delta P_{\mathrm{PFR}} + \Delta P_{\mathrm{FFR}}$, CPFE-Ref: $\hat{P} = P^* + \Delta P_{\mathrm{PFR}} + \Delta P_{\mathrm{FFR}}$

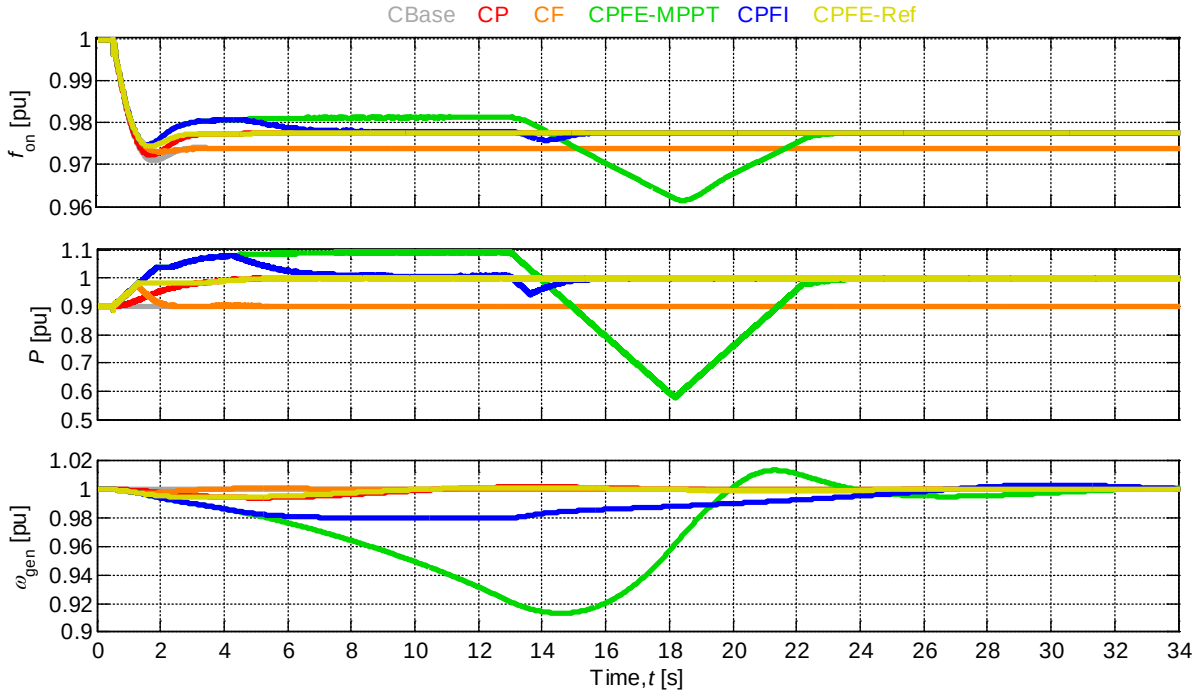

Figure 3-12: Case 12 – OWF's response to an onshore under-frequency event ($t = 0.5s$) at high wind speed – Reserves: 10% – Overloading released at $t = 13s$ – CBase: $\hat{P} = P^*$, CP: $\hat{P} = P^* + \Delta P_{\mathrm{PFR}}$, CF: $\hat{P} = P^* + \Delta P_{\mathrm{FFR}}$, CPFE-MPPT: $\hat{P} = P_{\mathrm{MPPT_0}} + \Delta P_{\mathrm{PFR}} + \Delta P_{\mathrm{FFR}}$, CPFI: $\hat{P} = P_{\mathrm{MPPT}} + \Delta P_{\mathrm{PFR}} + \Delta P_{\mathrm{FFR}}$, CPFE-Ref: $\hat{P} = P^* + \Delta P_{\mathrm{PFR}} + \Delta P_{\mathrm{FFR}}$

This project has received funding from the European Union's Horizon 2020 research and innovation programme under grant agreement No 691714.

3.2. ONSHORE POWER OSCILLATION DAMPING

Onshore power oscillations are triggered in the simulations by means of 1% load step changes (i.e., $\pm 16\ \mathrm{MW}/1600\ \mathrm{MW}$). The damping of such oscillations is decreased mainly by increasing the SG's AVR proportional gain. The OWF's response to such oscillations is illustrated in Figure 3-13, Figure 3-14 and Figure 3-15, for low, medium and high wind speeds, respectively. Each figure includes a base subcase response, corresponding to no contribution from the OWF in the damping of the onshore power oscillation. To improve the response, the POD control mode is activated at the next zero-crossing of the onshore power oscillation signal, ΔP_{on}, after the activation of the corresponding flag, F_{POD}, at $t = 0.3\ s$. As can be seen in all figures, the damping of the onshore power oscillations can be increased by having the OWF modulate P in response to the onshore signals directly communicated to it.

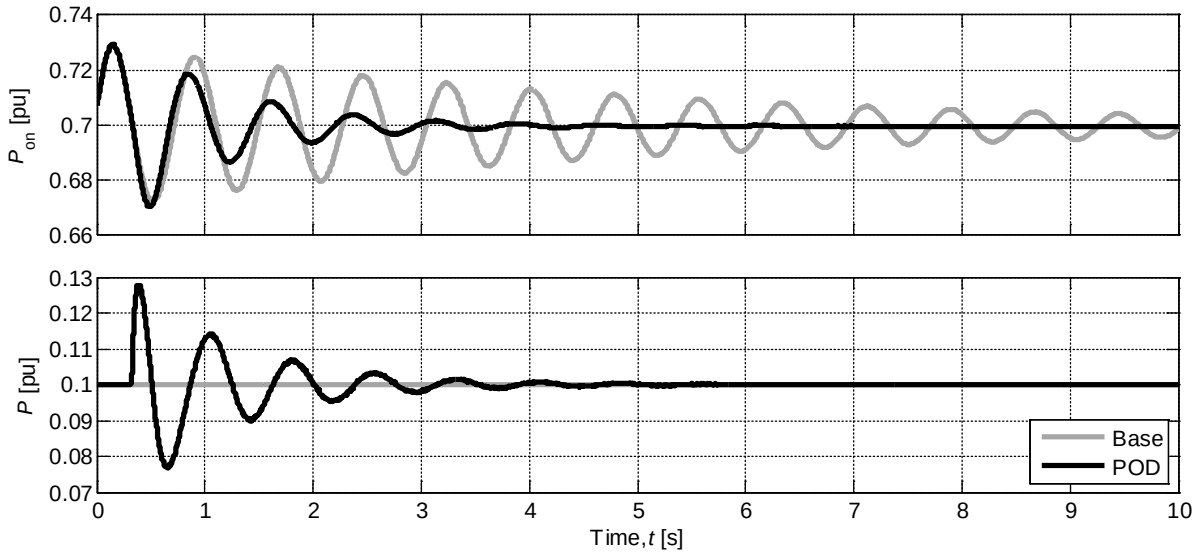

Figure 3-13: Case 13 – OWF's response to an onshore power oscillation at low wind speed

This project has received funding from the European Union's Horizon 2020 research and innovation programme under grant agreement No 691714.

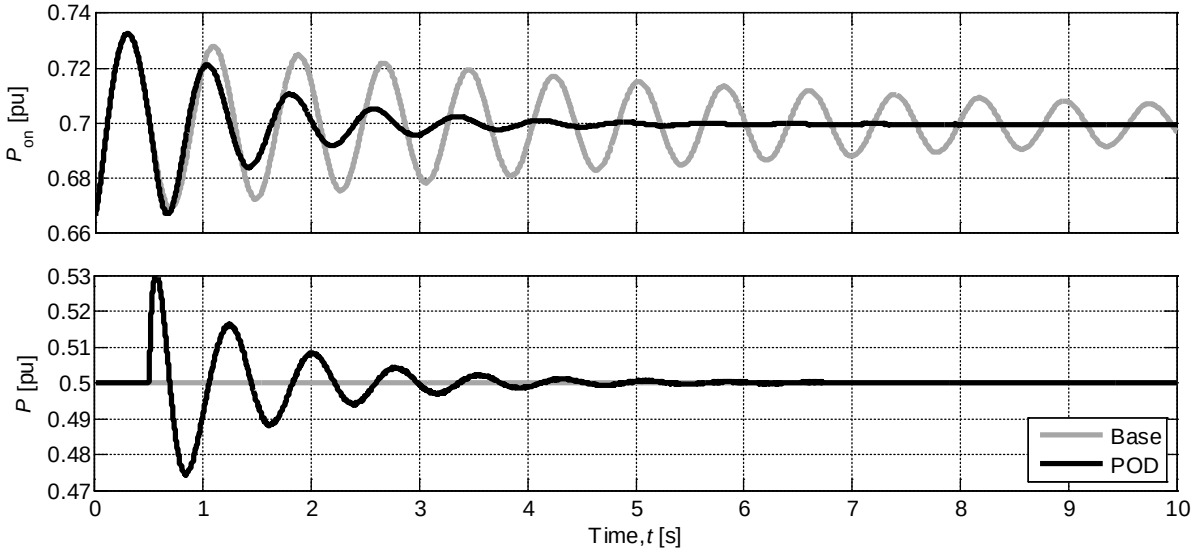

Figure 3-14: Case 14 – OWF's response to an onshore power oscillation at medium wind speed

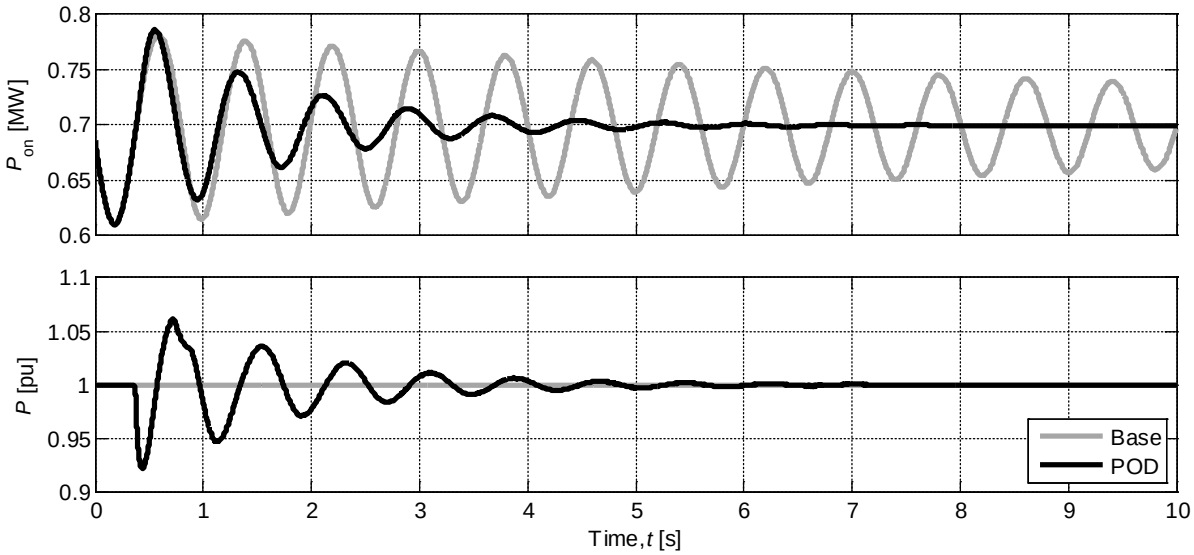

Figure 3-15: Case 15 – OWF's response to an onshore power oscillation at high wind speed

PROMOTiON - Progress on Meshed HVDC Offshore Transmission Networks

This project has received funding from the European Union's Horizon 2020 research and innovation programme under grant agreement No 691714.

4. CONCLUSIONS AND RECOMMENDATIONS

4.1. CONCLUSIONS

The simulation results suggest that—in principle—the new connection technology doesn't impact the capability of OWFs to provide FS and POD to onshore AC networks i.e., OWFs connected to HVDC via DRs can in principle provide such services by means of plant-level active power control strategies already developed for OWFs connected to HVDC via VSCs. In response to the corresponding onshore signals directly communicated to them, the OWFs can provide POD by modulating their active power output so as to produce damping torque onshore.

Such OWFs can deliver PFR during onshore frequency events, reducing the frequency deviation and maintaining it at a lower value for as long as the wind allows, also reducing the frequency nadir/zenith as a consequence. Moreover, preventively operating OWFs constantly curtailed can provide the additional active power needed for such response during onshore under-frequency events. The minimum production limit (e.g., 2.5%), imposed by the non-linear properties of the DRs, may, nevertheless, restrict such capability during onshore over-frequency events at low wind speeds.

The OWFs can also provide FFR, reducing the ROCOF just after the frequency event and the frequency nadir/zenith as a consequence. Such reduction, however, will be limited by the constraints imposed on the rate of change of the WT active power references. To further improve the frequency response, both PFR and FFR can be combined, and an additional constraint can be briefly applied on the rate of change of the active power reference to the WTs following the frequency nadir/zenith, on which the ROCOF changes sign.

By overloading their WTs, the OWFs can provide more than the available aerodynamic power (overproduce) for several seconds during an onshore under-frequency event. This, nonetheless, can result in a—possibly worse—new onshore frequency event during the recovery (underproduction) period. Moreover, it may even be unnecessary if active power reserves from curtailed operation are available, as such reserves may suffice for the provision of both PFR and FFR.

4.2. RECOMMENDATIONS FOR FUTURE WORK

Communication delays should be considered in future related studies. Just as similar studies previously conducted for the other connection technologies (i.e., AC, VSC-VSC-HVDC), the studies presented in this report should be extended to include several (aggregated) WFs/WTs/strings modelled in more detail.

This project has received funding from the European Union's Horizon 2020 research and innovation programme under grant agreement No 691714.

BIBLIOGRAPHY

S. I. Bernal-Pérez, “Integración híbrida multipunto en el sistema eléctrico de grandes parques eólicos marinos a través de redes de alta tensión en continua”, PhD thesis, Technical University of Valencia, Valencia, Spain, Nov. 2015.

S. I. Bernal-Pérez, S. C. Añó-Villalba, and R. M. Blasco-Giménez, “Stability Analysis of HVDC-Diode Rectifier Connected Off-shore Wind Power Plants”, in *Proceedings of the IEEE Industrial Electronics Society 41st Annual Conference (IECON 2015)*, Yokohama, Japan, 9th–12th Nov. 2015, pp. 4040–4045.

R. M. Blasco-Giménez, S. C. Añó-Villalba, J. Rodríguez-D’Derlée, S. I. Bernal-Pérez, and F. Morant-Anglada, “Diode-Based HVdc Link for the Connection of Large Offshore Wind Farms”, *IEEE Transactions on Energy Conversion*, vol. 26, no. 2, pp. 615–626, Mar. 2011.

ENTSO-E, “Network Code on HVDC Connections (HVDC)”, Network Code, Oct. 2015.

ENTSO-E, “Network Code on Requirements for Grid Connection Applicable to all Generators (RfG)”, Network Code, Apr. 2016.

S. Goumalatsos, “Investigation of Power Oscillation Damping service by offshore wind power plants connected via Voltage Source Converter High Voltage Direct Current link”, Master’s thesis, Technical University of Denmark, Lyngby, Denmark, Jun. 2014.

A. D. Hansen, M. Altin, I. D. Margaris, F. Iov, and G. C. Tarnowski, “Analysis of the short-term overproduction capability of variable speed wind turbines”, *Renewable Energy*, vol. 68, no. 1, pp. 326–336, Aug. 2014.

Hydro-Québec TransÉnergie, “Transmission Provider Technical Requirements for the Connection of Power Plants to the Hydro-Québec Transmission System”, Network Code, Feb. 2009.

National Grid Electricity Transmission, “The Grid Code – Issue 5, Revision 19”, Network Code, Sep. 2016.

PROMOTioN, “Deliverable 3.1: Detailed Functional Requirements to WFs”, Project Deliverable, Dec. 2016.

PROMOTioN, “Deliverable 3.2: Specifications of the control strategies and the simulation test cases”, Project Deliverable, Mar. 2017.

G. Rousi, “Methods for representations of wind farms in dynamic power system studies”, Master’s thesis, Technical University of Denmark, Roskilde, Denmark, Nov. 2013.

O. Saborío-Romano, A. Bidadfar, Ö. Göksu and N. A. Cutululis, “Frequency Support from OWFs connected to HVDC via Diode Rectifiers”, in *Proceedings of the 16th Wind Integration Workshop*, Berlin, Germany, 25th–27th Oct. 2017.

J. N. Sakamuri, A. D. Hansen, N. A. Cutululis, M. Altin, J. Sau-Bassols, E. Prieto-Araujo, and O. Gomis-Bellmunt, “Suitable Method of Overloading for Fast Primary Frequency Control from Offshore Wind Power Plants in Multi-Terminal DC Grid”, in *Proceedings of the IEEE PowerTech Manchester 2017 Conference*, Manchester, United Kingdom, 18th–22nd Jun. 2017.

G. C. Tarnowski, “Coordinated Frequency Control of Wind Turbines in Power Systems with High Wind Power Penetration”, PhD thesis, Technical University of Denmark, Roskilde, Denmark, Nov. 2011.

S. Wachtel, and A. Beekmann, “Contribution of Wind Energy Converters with Inertia Emulation to frequency control and frequency stability in power systems”, in *Proceedings of the 8th Wind Integration Workshop*, Bremen, Germany, 14th–15th Oct. 2009.

L. Zeni, “Power system integration of VSC-HVDC connected wind power plants, Control principles, power system services, clustering of wind power plants”, PhD thesis, Technical University of Denmark, Roskilde, Denmark, Mar. 2015.

This project has received funding from the European Union’s Horizon 2020 research and innovation programme under grant agreement No 691714.

L. Zeni, R. Eriksson, S. Goumalatsos, M. Altin, P. Sørensen, A. Hansen, P. Kjær, and B. Hesselbæk, 2016, “Power Oscillation Damping From VSC-HVDC Connected Offshore Wind Power Plants”, *IEEE Transactions on Power Delivery*, vol. 31, no. 2, pp. 829–838, Apr. 2016.

This project has received funding from the European Union's Horizon 2020 research and innovation programme under grant agreement No 691714.